JOURNAL OF PROPULSION AND POWER
Vol. 12, No. 6, November–December 1996

# High-Pressure Arc Heater Development and Modeling: Status and Requirements

E. J. Felderman,* R. Chapman,* J. L. Jacocks,† D. D. Horn,* and W. E. Bruce III‡
*Micro Craft Technology Arnold Engineering Development Center Operations, Arnold Air Force Base, Tennessee 37389*

**An arc heater development program has been undertaken to develop a large, high-pressure, high-power arc heater capability. A large, state-of-the-art segmented arc heater (H3) has operated successfully and is scheduled to be fully operational at chamber pressures up to 100 atm with a total power of 60 MW in 1996. The H3 arc heater is a 50% geometric scale-up of the existing H1 segmented arc heater and is designed to operate at 2.25 times the power of H1. Additionally, an extensive analytical capability to assist in the design and development of segmented arc heaters has been developed. Available modeling techniques are reviewed, current modeling efforts are discussed, and areas needing additional effort are identified. Scaling laws/performance correlations have been used extensively and first-generation performance codes have been available for some 20 years. The basic components of a three-dimensional arc heater code have been developed, extending a three-dimensional Navier–Stokes code by incorporating electromagnetic effects and a multidimensional radiation model. A near-electrode model has been developed for the interface between the flowing air and the solid electrode surface. Water-tunnel vortex-breakdown studies have been carried out to aid in understanding vortex behavior. Additional modeling work required to improve our understanding of arc heater phenomenology include continued development of the three-dimensional code, extension of the near-electrode model to include nonequilibrium effects, and improved modeling for arc path prediction.**

## Nomenclature

$a$ = speed of sound
$B$ = magnetic field
$c$ = speed of light
$E$ = electric field
$H_0$ = total enthalpy
$I$ = total current
$J$ = current density
$P_0'$ = pitot pressure
$Re$ = Reynolds number
$Re_m$ = magnetic Reynolds number
$T$ = temperature
$v$ = velocity
$\delta$ = divergence of magnetic field
$\mu$ = viscosity coefficient
$\mu_0$ = vacuum permeability
$\rho$ = density
$\sigma$ = electrical conductivity
$\sigma_{sb}$ = Stephan–Boltzmann constant

*Subscripts*
$m$ = magnetic component
$r$ = radiation component
$v$ = viscous component
$\infty$ = freestream conditions

## Introduction

ELECTRIC arc heaters have been used for aeronautical test purposes since the late 1950s, with the advent of long-range ballistic missiles and the associated need for testing of thermal protective materials for re-entry bodies. The high temperatures and pressures required for this type of materials testing, as well as other test requirements relating to structures and propulsion, are not attainable by conventional means. Electric arc heaters are the only viable method of heating air to high temperatures (2500–10,000 K) for a duration of several minutes. This is evident from the comparison of various types of test facilities presented in Fig. 1. Arc heaters have been developed and operated at the U.S. Air Force/Arnold Engineering Development Center (AEDC) since 1962. The nation's premiere high-pressure arc-heated facility (H1) was developed in 1976 and has been the workhorse facility for the past 14 years. The 50-MW Reentry Nosetip (RENT) Facility heater was relocated from Wright–Patterson Air Force Base (WPAFB) to AEDC in 1981 and is now the HR facility. The 50-MW High Temperature Leg (HTL) Facility was relocated from WPAFB to AEDC in 1986 and is now the H2 facility.

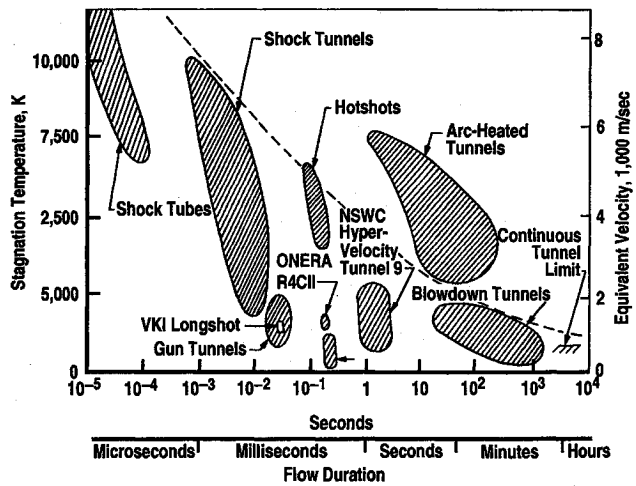


**Fig. 1 High-temperature tunnel capabilities.**

Received Nov. 2, 1994; revision received Feb. 15, 1996; accepted for publication Aug. 17, 1996. 

*Principal Engineer, Facility and Space Technology Department. Member AIAA.
†Executive Engineer, Computational Fluid Dynamics Department.
‡Senior Engineer, Facility and Space Technology Department.

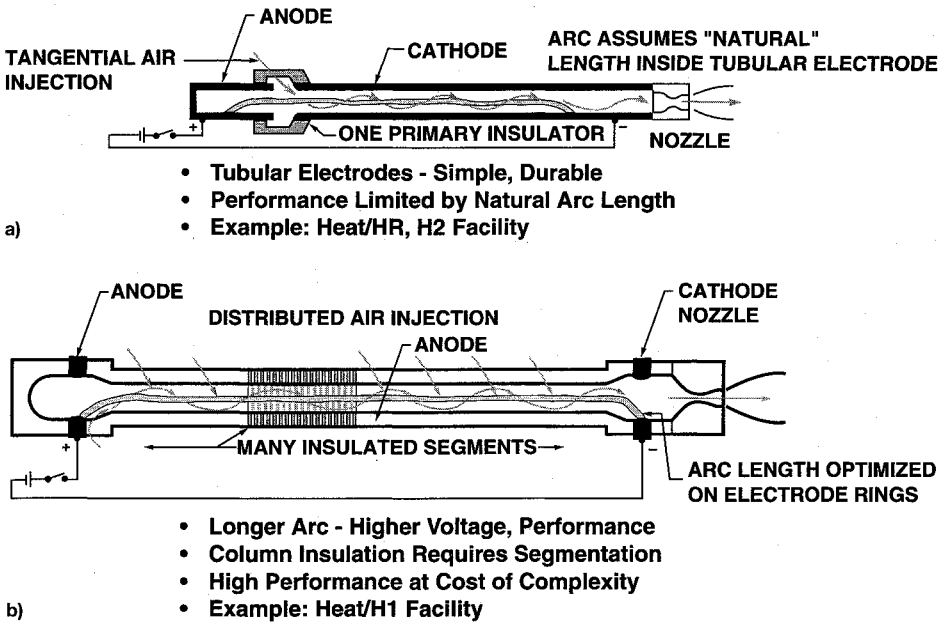


**Fig. 2 Basic arc heater types: a) Huels and b) segmented.**

The HR and H2 test units utilize a conventional Huels-type arc heater consisting of two coaxial tubular electrodes separated by a swirl chamber, as shown in Fig. 2a. The Huels-type heaters are characterized by simplicity, reliability, and operational maturity, but limited performance. The H1 test unit utilizes a segmented arc heater having approximately 200 electrically isolated segments separating the anode (upstream end) and cathode (nozzle end), located at opposite ends of the heater, as shown in Fig. 2b. The segmented arc heater offers not only higher pressure and enthalpy capability, but also much less contamination from electrode erosion, since it operates at higher voltage and lower current. The HR facility also has a semicircular nozzle with a flat lower surface that can be used to test large, flat material samples. Flared nozzles that are available in the H1 and HR facilities produce a continually expanding flowfield and a continuously varying impact pressure with axial distance from the nozzle exit. Through continuing upgrade efforts, operation of the H1 heater at a chamber pressure up to 150 atm has been demonstrated and various arc heater diagnostic experiments have been performed. Results from several of the arc heater diagnostic experiments are presented in Ref. 1. An aggressive analytical effort has been ongoing for several years to address such technical issues as arc stability and reliability, electrode erosion, flow quality, scaling parameters, throat cooling, wall heat flux, and pressure containment. The arc facilities produce the high heating, pressure, and shear conditions encountered during re-entry and hypersonic flight, so that flight materials can be tested for time periods close to flight heating times. Run time at maximum enthalpy is approximately 2 min for the Huels-type heater and approximately 1 min for the segmented heater. The primary factors limiting run time are electrode life and power supply limits. The aerothermal performance of the three arc facilities is presented in Fig. 3.

### Test Facility Simulation of Flight Conditions

For materials and structures testing, the simulation methodology usually involves matching $P'_0$, and $H_0$, without regard to how it is distributed between static enthalpy and kinetic energy. A consequence of this procedure is that the Mach number is not duplicated. This methodology is often depicted on an altitude–velocity map, as shown in Fig. 3. Historically, the AEDC arc facilities have been heavily utilized to simulate intercontinental ballistic missile (ICBM) trajectories, especially the maximum heating area as noted in Fig. 3. The opposite of

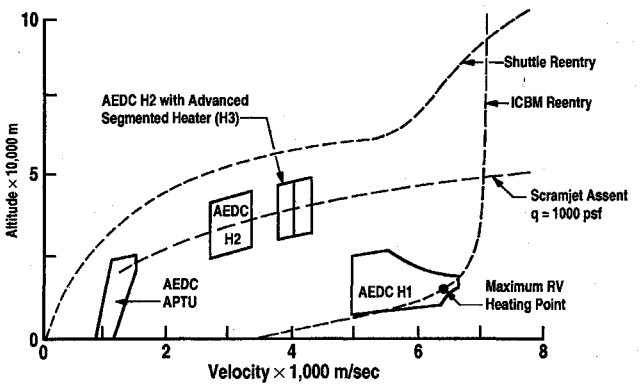


**Fig. 3 Heating rate simulation envelopes.**

a very steep re-entry (ICBM) is a shallow re-entry such as the shuttle trajectory also shown in Fig. 3. The NASA Ames Research Center has been active in simulating the high-velocity portion of the shuttle trajectory. The potential scramjet propulsion corridor lies midway between these two extremes. The simulation requirements for propulsion testing are much more stringent, essentially requiring complete flight duplication. As a result, much scramjet testing may have to be done in the direct-connect mode, where combustor entrance conditions are duplicated, as opposed to simulation of the engine inlet condition.

### Future Requirements

Hypersonic testing requirements for propulsion, materials, and structures presently exceed national testing capabilities. Larger, higher performance arc heaters are required to meet the testing needs, particularly for hypersonic airframe structures and propulsion systems above Mach 8. The current scramjet capability in the H2 facility is discussed in Ref. 2. A larger flowfield is required to accommodate large components such as radomes, sensor windows, and control surfaces of hypersonic glide vehicles. Aerothermal testing also requires long run time and high enthalpy. Higher pressures are required for leading edge, nosetip, and propulsion testing. These improvements in test facility capabilities will only become more critical for future hypersonic testing requirements. The current AEDC development effort is aimed at extending the size and performance of arc heaters to satisfy more of the potential hypersonic testing needs.

## AEDC Development Plan

The initial goal of the AEDC arc heater development plan is the development of a larger arc heater, H3, designed to operate at approximately 2.25 times the power of H1. Next, the plan will focus on increasing the operational pressure of segmented arc heaters and apply this technology to the H3 heater. Future arc heater development programs will rely heavily on the experience with the H3 development effort. An important feature of the AEDC plan is to incorporate interim improvements into the existing aerothermal test facilities. H3 will be used in place of H1 or HR to allow the testing of larger models and material samples. H3 will also be installed in the H2 facility to extend the capability of H2 to higher pressure, enthalpy, and power.

### Large Arc Heater Development: H3

AEDC is focusing on the development of the segmented-type arc heater over the Huels-type heater because of the improved performance and flow quality of a segmented heater over the Huels-type heater. The H1 heater was used as the starting point to expand the segmented arc heater technology base. Knowledge gained from experience with the H1 heater and results from analytical modeling efforts have been incorporated into the H3 heater design and will be used during the development of the H3 heater. Specifically, the H1 heater was used to address scale-up issues such as arc stability, operational reliability, air injection configuration, power supply interaction, electrode erosion, flow quality, bore length-to-diameter ratio, throat-to-bore diameter ratio, and scaling relations.

The H3 arc heater presently under development is shown in Fig. 4, prior to the connection of the air and cooling water hoses. The H3 heater is basically a 50% geometric scale-up of the H1 segmented heater[3] and is designed to operate at 80 MW; however, the present power supply will limit H3 operation to approximately 60 MW. The H3 heater is designed as a pressure vessel for 200 atm with an operational pressure of 150 atm. The heater has a bore diameter of 7.62 cm (3 in.) and the water-cooled copper electrodes are 11.4 cm in diameter, with the anode located upstream and the cathode downstream similar to H1. Four nozzles have been designed (see Table 1). The 3.43-cm nozzle throat diameter corresponds to the 50% scale-up of the standard H1 nozzle throat diameter of 2.88 cm. In the heater bore, each group of 18 segments are bound together into a module to simplify assembly and disassembly of the heater. The heater can be assembled using 8, 10, or 12 modules. The 12-module configuration corresponds to the 50% geometric scale-up of H1. The total heater length from end flange to nozzle flange is 3.35 m.

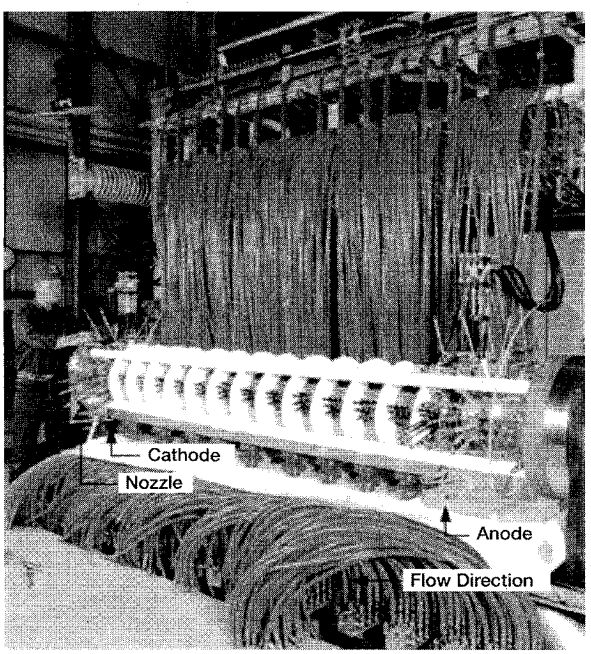


Fig. 4 H3 arc heater.

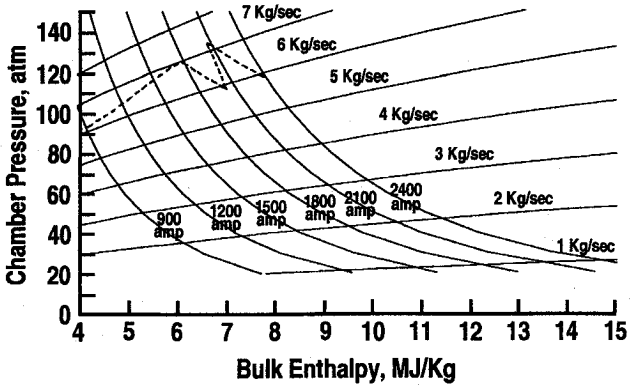


Fig. 5 H3 pressure–enthalpy envelope with 3.43-cm-diam throat.

Air is injected tangentially into the heater at both electrodes and between segments in the heater bore. A special mixing-air section has been designed and fabricated to be installed downstream of the cathode to provide the capability for injection of cold air to lower the total enthalpy. The cold air mixing section has the capability to inject up to 68% of the total airflow.

Magnetic coils are located in the housing of each electrode to assist the arc attachment positioning and rotation. Initial coil configurations were determined based on experience with H1 and analytical work performed at AEDC.[4] The coil configuration can be quickly and easily changed using connectors external to the heater. The electrode liners are easily removed from the housing for replacement.

The performance envelopes for H3 have been estimated using empirical scaling relations derived from data of three high-pressure segmented arc heaters. The projected chamber pressure and bulk (mass-averaged) enthalpy envelope with lines of constant current and mass flow rate is shown in Fig. 5 for the 3.43-cm-diam nozzle throat.

The H3 heater has the same pressure–enthalpy envelope as the H1 arc heater; however, the H3 heater will provide a 50% larger diameter flowfield at 2.25 times the mass flow rate and power, which will allow the testing of larger models. The issue of arc heater flowfield contamination from electrode erosion has been a concern to the hypersonic testing community, particularly for propulsion testing. Studies have found that the level of contamination from the AEDC H1 segmented heater has a negligible effect on most types of hypersonic testing.[5] The H3 arc heater is expected to have the same low contamination concentrations as H1.

Upon completion of development, the H3 heater is initially planned to be installed in the H2 facility to replace the existing Huels-type heater to improve the facility performance. The H3 heater will improve the pressure, enthalpy, power, and air mass flow rate in the H2 facility. The projected improvement in the enthalpy–pressure envelope for the H2 facility with the H3 heater and a 3.81-cm-diam nozzle throat, is shown approximately in Fig. 3.

### High-Pressure Arc Heater Development

The H1 arc heater will be used as the starting point for additional high-pressure arc heater development. The H1 segmented arc heater was designed as a pressure vessel for 200 atm, although the operating design point was 150 atm. As early as 1979, the heater was operated at a pressure of 160 atm and 22.5-MW power with no indication of damage from pressure. In 1987–1988, three runs at 150 atm and 30 MW were completely successful. The initial goal was to develop the H1 heater to an operational pressure of 250 atm. Experience gained with the 250-atm development effort will be used to

assist in the development to even higher operating pressure (~400 atm). The knowledge gained from the H1 high-pressure development effort will be applied to the H3 arc heater.

The 250-atm operating pressure goal is not a reflection of flight duplication requirements (which are much higher), but rather represents a realistic appraisal of the difficulty in design of an elongated pressure vessel, electrically insulated from end to end, and subject to a 57-MW/m$^2$ heating rate on the inside wall.

### Manifolding Experiments

Future AEDC plans include the development of a larger arc heater capability than H3 (currently under development), either by developing a new even larger heater or manifolding several H3-size heaters into a common plenum, as illustrated in Fig. 6. Such multiarc configurations can be a convenient route to higher power heaters, but at somewhat reduced performance because of additional wall cooling losses. A multiarc configuration may also be an effective way to improve the flow uniformity of both enthalpy and pressure. The mixing of effluents of separate arc heaters in a single plenum may dampen flowfield fluctuations because oscillations in the individual arc units will probably be independent. A smaller scale multiarc installation is operational at Aerospatiale in Bordeaux, France. Investigations are currently underway to better document energy losses and flowfield quality. Data have been obtained and preliminary analysis indicates that losses are not prohibitive and flow quality is at least as good as single arc installations. In the continuing data analysis, flowfield data from the Aerospatiale multiarc facility will be compared with data from the single-arc facility to evaluate the improvement in flowfield fluctuations and profile. The overall thermal efficiency of the multiarc manifold system will also be evaluated.

### Additional Development Efforts

Several other activities are being pursued by AEDC in coordination with other contractors relative to arc heater development. Internally water-cooled enthalpy and pitot-pressure probes with the capability to dwell on the flowfield centerline are presently being developed. Prior to this development effort, all arc facility diagnostic probes were swept through the flowfield, giving a transient profile of the flow.[6] The new probes are designed to obtain steady-state enthalpy and pressure data in the flowfield. The enthalpy probe uses a double sonic orifice technique to determine the flowfield enthalpy.[7] Both probes use diffusion-bonded foil construction to form the internal cooling water passages. Two small contracts to investigate the possibility of coating arc heater segments with a high-thermal-conductivity, high-electrical-resistance material have been funded. If segments can be coated with such a material that would withstand the severe arc heater environment, the arc stability in the heater would be improved by reducing the possibility of damage to the segments from arc breakdown and conduction along the constrictor wall.

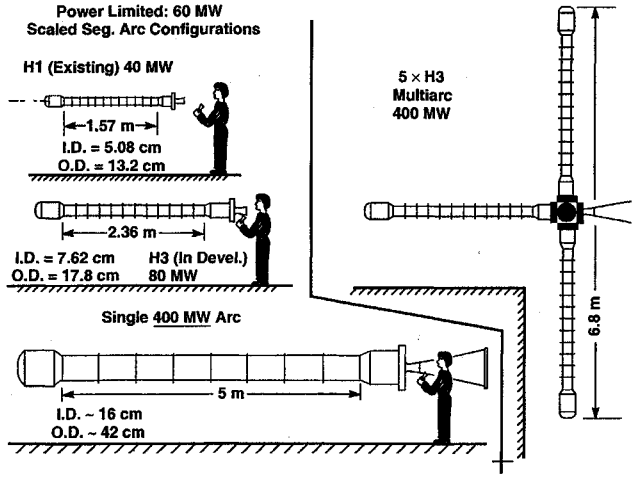


**Fig. 6 Single-arc vs multiarc configurations.**

## Modeling Capability

An extensive analytical capability has been developed to assist in the design and development of segmented arc heaters. Existing analytical tools, those currently under development, and the unfilled modeling requirements will be discussed in the following text.

### Scaling Laws

The internal flowfields of arc heaters, which are characterized by embedded regions of intense thermal energy release in an electric discharge, have proven to be difficult to calculate without substantial simplifying assumptions. Several analysis methods have been developed, but comparisons of solutions with experimental measurements on existing arc heaters have met with only partial success. Historically, the process of scaling arc devices to larger size has relied as much upon empirical scaling relations as upon results of analytical calculations. Relatively simple and easy-to-use scaling relations between electrical, thermal, and geometric variables have been developed by straightforward regression of experimental databases. Recently, such relations have been put on a nondimensional basis by incorporating dimensional analysis in the database regressions.[8] However, limitations on possible measurements in arc heaters necessitated modification of classical dimensional analysis by analytical additions to the experimental data of postulated profiles of enthalpy, which conform to the fundamental laws of conservation of mass, energy, and electric current.

### First-Generation Codes

The ARCFLOW computer code was developed by NASA Ames Research Center and was modified for high-pressure applications nearly 20 years ago.[9] By adding a swirling flow capability it was substantially improved in 1978 and renamed SWIRLARC.[10] The code has several shortcomings as stated in the following text, but does a reasonable job of predicting overall operating parameters, even though the assumptions noted prevent accurately modeling the details of the flow inside the arc heater and limit the application of the code to the constrictor region. The solution algorithm is explicit. The flow is assumed to be steady, axisymmetric, and in local thermodynamic equilibrium at the heavy gas temperature. A quasicylindrical assumption is imposed (boundary-layer-type flow) and the resulting radial momentum equation inadequately represents the flowfield. The radial velocities in the tube are assumed to be much smaller than the axial or circumferential velocities, and the gradients in the radial direction are assumed to be much stronger than those in the axial direction. The quasicylindrical conditions imply weak swirl; for strong swirl, reverse flow can exist in regions of low axial velocity, thus violating the previous assumptions. The electromagnetic effects, which are so important in the arc heater phenomenology, are not adequately taken into account. The electric field is assumed to be constant along the constrictor axis and the induced magnetic field is ignored. Thus, the Lorentz force and the magnetic field contribution to the current are neglected. The radiation model is a one-dimensional, analytical, gray-gas emission–absorption model, i.e., gradients along the constrictor axis are not considered. The assumed initial enthalpy profile must contain a significant portion of the final energy, as opposed to nearly all of the energy being added to the gas by Joule heating in the arc, for the code to run.

Direct evidence of arc fluctuation from the centerline has been obtained by optical imagery of the arc during heater operation. An example of this is shown in Fig. 7. Windows were positioned at three axial locations along the constrictor wall.

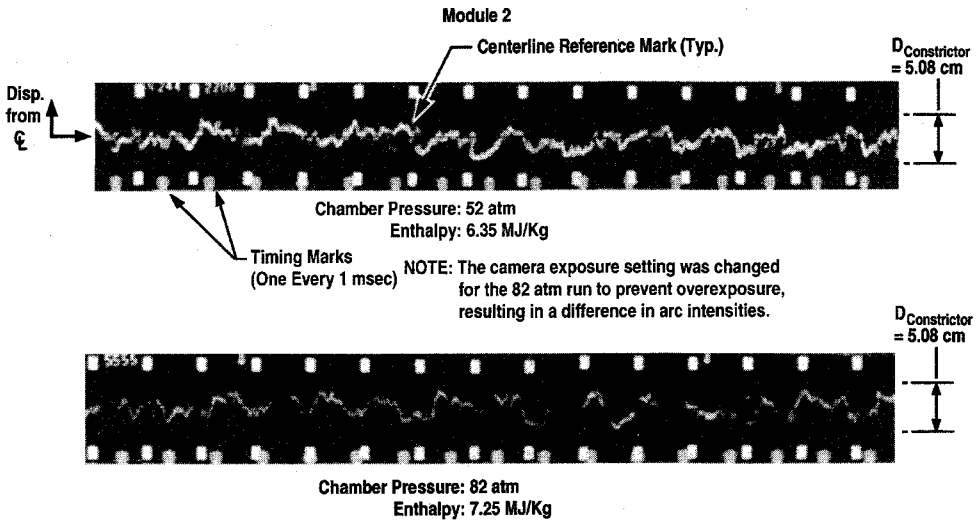


**Fig. 7 Arc stability observations using segment sidewall port at two operating conditions.**

The arc displacement from the centerline is shown as a function of time (at one axial window location) in Fig. 7. In this figure, displacements of the arc column away from the heater axis are recorded photographically as displacement perpendicular to the direction of motion of the high-speed film strip. Dominant oscillations with displacements that extend over a large fraction of the heater inside diameter occur at a frequency somewhat less than 1 kHz, whereas smaller oscillations occur at frequencies greater than 1 kHz. This indicates a need for a multidimensional radiation model in any three-dimensional code that purports to realistically model the flow.[11]

### Three-Dimensional Arc Heater Code (XLIM3D)

Improved analytical tools must be developed that eliminate many of the shortcommings referred to previously before we can improve the operational reliability of existing arc heaters and have confidence in our ability to design and scale new arc heaters. Because of the complex nature of arc heaters, a three-dimensional model is required. A computer code, XLIM3D, is currently under development to support the arc facilities. XLIM3D is a flexible computational fluid dynamics-type program that is built upon a three-dimensional, thin-layer, Navier–Stokes code written by Reddy and Benek.[12] The code has been extended to incorporate the electromagnetics and radiation along with the fluid dynamics through the addition of separate modules containing the electromagnetic and radiation transport equations.[13] Solutions to the combined field (i.e., fluid dynamics, electromagnetics, and radiation) calculations are found by iteration of the individual solutions for the modules obtained using a locally implicit algorithm. The developmental approach was to initially employ a time-dependent, three-dimensional, single-temperature, single-fluid, equilibrium magnetohydrodynamic (MHD) formulation for simplicity. Later, the code will be extended to a multitemperature, multifluid, nonequilibrium electromagnetohydrodynamic (EMHD) formulation.

*Fluid Dynamic Equations*

Currently, the fluid dynamics are described by a single set of mass, momentum, and energy equations. The model treats the plasma as a single-temperature fluid. The nondimensionalized, time-dependent, Reynolds-averaged Navier–Stokes equations can be expressed in Cartesian coordinates as

$$\frac{\partial Q}{\partial t} + \frac{\partial}{\partial x}(E - E_v) + \frac{\partial}{\partial y}(F - F_v) + \frac{\partial}{\partial z}(G - G_v) = 0$$

where $Q$ contains the conservative variables for mass, momentum, and energy; $E$, $F$, and $G$ are the components of the flux vector; and $E_v$, $F_v$, and $G_v$ are the viscous terms. The velocity components are nondimensionalized by the freestream sound speed $a_\infty$, the density by the freestream density $\rho_\infty$, and the total energy by $\rho_\infty a_\infty^2$. The Reynolds number is given by

$$Re = \rho_\infty a_\infty / \mu_\infty$$

where $\mu_\infty$ is the freestream viscosity coefficient. The flow is assumed to be air in thermal and chemical equilibrium. The thermodynamic and transport properties such as pressure, temperature, thermal conductivity, and viscosity are obtained from the curve fits of Srinivasan et al.[14,15] for equilibrium air. Also, the code can be run for a perfect gas if desired.

The turbulent viscosity is computed by the Baldwin–Lomax turbulence model[16] or a low-Reynolds number $k$-$\varepsilon$ turbulence model developed by Nichols.[17] The two-equation $k$-$\varepsilon$ turbulence model has been incorporated to better model recirculating flow. The time-dependent equations for turbulent kinetic energy and dissipation are solved in a decoupled mode from the Navier–Stokes equations, lagged by one time step. The Navier–Stokes equations are transformed into general curvilinear coordinates and the thin-layer approximation is made.

*Electromagnetic Equations*

Currently, the electromagnetics are described by the magnetic induction equation. The plasma is assumed to be quasi-neutral. The nondimensionalized, time-dependent electromagnetic equations can be expressed in Cartesian coordinates as

$$\frac{\partial Q_m}{\partial t} + \frac{\partial E_m}{\partial x} + \frac{\partial F_m}{\partial y} + \frac{\partial G_m}{\partial z} = 0$$

where $Q_m$ contains conservative variables for the magnetic field and $E_m$, $F_m$, and $G_m$ are the components of the magnetic field flux vector. The Lorentz force and Joule heating terms are added to the momentum and energy equations, respectively. The velocity components are again nondimensionalized by $a_\infty$ and the magnetic field by $\mu_0 I$. A term $-\delta$, where $\delta = \nabla \cdot B = 0$, is inserted into the formulation along the diagonal of $E_m$, $F_m$, and $G_m$, which drives $\delta \to 0$ and ensures that $\nabla \cdot B = 0$ will not be violated. The current density is related to the electromagnetic fields by a general Ohm's law of the form

$$J = \sigma(E + v \times B)$$

Hall effects are ignored since the Hall parameter is on the order of $10^{-5}$ at the arc core for typical arc heater conditions. The magnetic Reynolds number is given by

$$Re_m = \sigma \mu_0 a_\infty$$

and is typically on the order of 5 $m^{-1}$. The electrical conductivity is obtained from curve fits for equilibrium air, which are derived from a collisional model developed by Nicolet et al.,[9] and is typically on the order of 11,500 Ω/m. By comparison, the classical Spitzer–Harm conductivity for a fully ionized plasma is on the order of 10,900 Ω/m. The magnetic induction equation is also transformed into general curvilinear coordinates.

*Radiation Transport Equation*

The radiation is described by the diffusion model of radiation. This model is based on the gray gas and Milne–Eddington approximations and is valid for high pressures. The nondimensionalized, time-dependent radiation transport equation can be expressed in Cartesian coordinates as

$$\frac{1}{c}\frac{\partial Q_r}{\partial t} + \frac{\partial E_r}{\partial x} + \frac{\partial F_r}{\partial y} + \frac{\partial G_r}{\partial z} = S$$

where $Q_r$ contains the conservative variable for radiation intensity; $E_r$, $F_r$, and $G_r$ are the components of the radiant heat flux vector; and $S$ is the radiation source term. The divergence of the radiant heat flux vector is added to the energy equation. The radiation intensity is nondimensionalized by $\sigma_{sb} T_{ref}^4$, where $T_{ref}$ is an arbitrary reference temperature.

This form of the radiation transport equation obviates the necessity of performing geometric integrations, instead, an integration in time of the scalar radiation intensity is performed. The absorption coefficient is obtained from curve fits for equilibrium air that are derived from a band-weighted model developed by Nicolet et al.[9] as reported by Shaeffer.[10] The radiation transport equation is also transformed into general curvilinear coordinates.

Felderman and MacDermott[11] have used this radiation model to estimate the increase in the local radiative heating of an arc heater wall caused by arc displacement from the centerline of the magnitude observed in Fig. 8. A radiant flux calculation using a temperature profile displaced from the centerline at an amount equal to 40% of the radius is compared to a symmetric calculation in Fig. 8. The radiant flux incident on the near wall is increased while that on the far wall is decreased. The circumferential distribution of the wall heat flux is shown in Fig. 8; the relation between the location of the maximum flux at the wall and the temperature peak is readily apparent. An unsteady conduction heat transfer analysis of the water-cooled constrictor wall was also reported in Ref. 11. At the arc fluctuation frequencies observed, the wall is not in danger of a burn-through failure, even though the wall would fail if continuously exposed to the maximum heating rates.

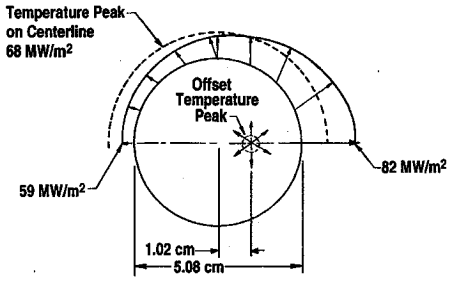


**Fig. 8 Radiation wall heat flux distribution in long circular cylinder, asymmetric temperature distribution.**

*Solution Algorithm*

The equations are solved using a locally implicit algorithm originated by Reddy and Jacocks[18] for solving three-dimensional compressible Navier–Stokes equations in complex flow domains. The locally implicit method (LIM) is based on a point relaxation scheme applied to the nonlinear equations that result from discretization of the equations. It does not require linearization of the equations and is completely matrix-free, thus avoiding the computationally expensive evaluation of Jacobian matrices. The algorithm has the good stability characteristics associated with implicit schemes, while retaining the computational simplicity of the explicit schemes. It can easily accommodate auxiliary equations and source terms do not effect the solution accuracy. Also, it is amenable to vector and parallel processing, unstructured grids, and/or domain decomposition techniques. Complex flow problems are solved by incorporating the algorithm into the chimera scheme developed by Benek,[19,20] which is a domain decomposition/grid embedding procedure with proven capability.[21]

Smoothing is implemented for the fluid dynamic equations for numerical stability, whereas smoothing is not used for the electromagnetic and radiation transport equations. The second-/fourth-order dissipation model of Jameson et al.,[22] as modified by Swanson and Turkel,[23] is used in the implicit inner iteration, and total variation diminishing (TVD) smoothing is used in the explicit point updates.

*Boundary Conditions*

Boundary conditions are implemented in a manner consistent with the locally implicit approximation. Values of the conserved variables are updated at the beginning of every sweep through the mesh. This approach propagates the boundary influence through the computational domain as rapidly as possible consistent with the method. Therefore, all points of the mesh are treated with the same degree of local implicitness.

The thermal boundary conditions at the wall may be either adiabatic wall or specified wall temperatures. The flow boundary conditions at the wall may be either inviscid or viscous. For inviscid boundaries, the contravariant normal velocity is set to zero and the other quantities are extrapolated from the interior. For viscous boundaries, the no-slip condition is applied on the velocity vector and density and pressure are extrapolated from the interior. For inflow boundaries, two types of Riemann invariants are available. One involves the free-stream Mach number and the other assumes isentropic flow from specified stagnation conditions. Both generally extrapolate values from the interior of the computational domain. Alternatively, the inflow boundaries may be specified. For outflow boundaries, subsonic flow uses specified pressure and extrapolation of the other quantities from the interior, whereas supersonic flow uses extrapolation of all the quantities from the interior.

The boundary conditions for the induced magnetic field are related to the current flux at the electrodes and insulators through Maxwell's equations. The electrode boundaries use specified current magnitude, with the flux constrained normal to the surface. The insulator boundaries use the normal component of the current flux set to zero. Applied fields are additive to the induced field at the boundaries. The radiation boundary condition at the wall is assumed to be that of a blackbody.[24]

*Status*

The status of the code development is that the modules (fluid dynamics, electromagnetics, and radiation transport) have been installed and validated individually for sample problems. However, solutions for the combined field calculations have not yet been attained. The code is well proven to be robust and efficient in obtaining solutions of the fluid dynamic module.[11] The capability in computing swirling, recirculating flow has been demonstrated by comparison with the data of Vu and Goul-

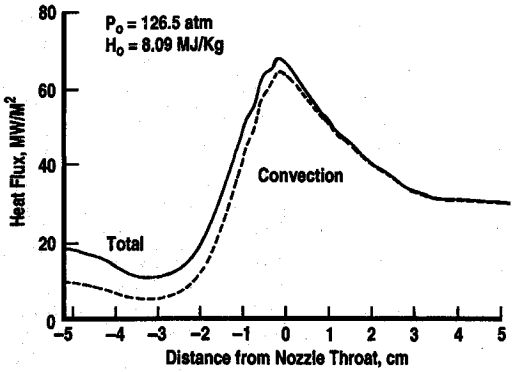


**Fig. 9 Nozzle throat heat transfer computed with XLIM3D code.**

din.[25] Validation of the radiation module was accomplished by comparison with the previous results of Nicolet et al.[9] The electromagnetic module has been validated for simple sample problems. However, work remains to be done to enable solutions to geometrically complex, fully coupled fluid dynamic and electromagnetic problems. An example of the application of the fluid dynamics and radiation transport sections of the code is given in Fig. 9. The heat flux to the wall of the H1 Mach 1.8 nozzle is shown as both the conduction and conduction plus radiation. Note that the radiation becomes negligible downstream of the throat, but is the major heat load upstream. The code predicts that the radiation flux increases with increased pressure and size.

### Near-Electrode Model

An understanding of the detailed physics of the discharge in the immediate region around the attachment to the electrode surfaces, where there is a rapid transition from gaseous to solid state conduction of electrical current, is key to understanding such issues as electrode survivability and electrode erosion. A comprehensive model for the near-electrode region at high pressure, extending from the flow region all the way into a copper electrode, has been presented in Ref. 26. The approach differs significantly from those previously reported. The concept of a space-charge sheath (which is a zero or low current model), is replaced with a thicker, continuum region, which is referred to as a current concentration zone.

It has long been observed in a wide range of arc devices that under certain conditions electrical current concentrates in the near-electrode region; the current density in the outer flow is much lower than at the spot where it enters the electrode. A linear variation in conduction area is assumed; since the thickness of the region is a product of the solution, this assumption does not drastically affect the final result. The implied variation in current density is imposed on the joule heating term in the heavy gas energy equation. This results in a drastically increasing heat flux as the wall is approached. The recent study analyzes the near-electrode region for air at higher pressures (100 atm) than considered in prior analyses. The high pressure assures the validity of the continuum approach; some nonequilibrium ionization is still present at high pressure, although not as much as would be expected at lower pressures. A field emission boundary condition is used at the cathode and a nonequilibrium electron temperature is incorporated at the anode. A one-dimensional gas-phase analysis is linked to the three-dimensional solid (or liquid) heat conduction zone beneath the electrode surface for a rapidly moving arc spot (typically 60 m/s). The near-electrode region is a very thin region compared to the flow region, and hence, the flow velocity in this region is considered negligible. The solution to the conservation equations thus reduces to a heat conduction problem. The region is divided into four subregions or zones. Starting from the flow side the zones to be considered are: the flow region, the current concentration zone, the work function, and the solid state heat conduction zone.

Simultaneous solutions satisfying gas phase calculations in the first two zones and the solid state in the last two zones were obtained for a given total current of 1000 A and gas static pressure of 100 atm. Using wall current density as a parameter, values of wall heat flux and temperature were obtained.[26] Repeating this process for other current densities (i.e., spot sizes) and allowing for the work function, results in the definition of cathode and anode operating lines. When boil-off mass loss rates predicted for these conditions are compared with measured electrode mass losses, we find the projected operating range can be narrowed to 3800–4400 K for a cathode spot and 4100–4600 K for an anode spot. The predicted spot sizes are consistent with observations.

### Vortex-Breakdown Studies in a Water Tunnel

A confined vortex flow is used inside the high-pressure arc heater to stabilize the arc discharge at an ideal safe location on or near the heater axis. Numerous parameters affect the arc and vortex core position along the length of the arc heater. Unfortunately, there are certain conditions under which decreasing stability of the vortex flow may lead to a vortex burst, a breakdown of the structured flow. To provide insight into this phenomena, Vakili[27] has performed qualitative and quantitative studies of forced swirling flows produced in a water-tunnel model of the AEDC H1 heater. Many investigations of vortex breakdown have been made,[28] but there is still no universal or generally agreed upon variable that can be categorically related to breakdown. Most of the studies are in agreement that stability, adverse pressure gradient, and a process analogous to the hydraulic jump are primary parameters influencing vortex burst. Extensive experimental and theoretical work has been performed in studies on vortex dynamics using both air and water as a medium. Khorrami and Grosch[29] found that instability growth rates were much greater in two-cell vortex structures (where reverse flow is present) than in single-cell vortices. Vakili and Eramo[30] demonstrated a strong coupling between external fluidic periodic forcing and vortex stability in a single-cell environment. Understanding the influence of vortex structure on the stability of vortices has, as a prerequisite, a reasonable understanding of the steady-state characteristics of the multicell vortex. The water-tunnel experiments are the first step in acquiring that understanding by observing details in such flows. Water-tunnel experiments at high Reynolds numbers ($10^4$), exhibited a gently meandering three-cell vortex flow. For low Reynolds numbers ($5 \times 10^3$), flow in most of the constrictor was dominated by a single-cell vortex. The Burgers model reasonably predicts the flowfield for the low-flow rate case where the entire flowfield is single cell.[31] It is a measure of the current heavy reliance on empiricism in this area that, presently, no theory exists in the open literature for predicting the existence, much less the velocity field, of a three-cell vortex flow. Of particular interest in the vortex core burst studies were those excitations that enhanced the flow structure under adverse conditions, and those that destroyed the vortex in otherwise favorable conditions. It was found that this forced swirling flow was quite susceptible to radial disturbances.[27] While the analogy between the water tunnel and the arc heater is far from complete and vortex behavior in the high enthalpy flow could be significantly different, the water tunnel work is an important step in understanding how vortex breakdown influences the arc path in a vortex-stabilized arc heater.

## Modeling Needs

### Mature Three-Dimensional Arc Heater Code

Further work is required and an effort is underway to enable solutions of the combined field calculations (fluid dynamics, electromagnetics, and radiation transport) with the present version of the code. However, several of the assumptions used in

a single-temperature, single-fluid, equilibrium MHD formulation severely limit the applicability of the code, and future work involves ultimately extending the code to a multitemperature, multifluid, nonequilibrium EMHD formulation. Recently, some of these limitations have been addressed by various code developers for arcjet and magnetoplasmadynamic thruster applications.[32-36]

The electromagnetic equations would be recast in terms of the time-dependent equations for both the electric and magnetic fields. This approach, which is commonly used in computational electromagnetics (CEM) (e.g., Shankar et al.[37]), would give a more accurate and complete electromagnetic description while enabling the modeling of high-frequency or short-time-scale phenomena. It would also greatly simplify implementation of the boundary conditions.

A separate set of fluid dynamic equations to model the electrons would be added. This would allow for thermal and ionization nonequilibirum, which is inherent in all electrically driven plasmas and for charge separation that is necessary to model the electrode sheath regions. Finite rate chemistry would be addressed by inclusion of the NEQPAK package developed by Curtis,[38] which provides chemical, thermodynamic, and transport properties for high-temperature reacting flows and allows for thermal nonequilibrium, multitemperature reaction models. It will also be necessary to extend NEQPAK to include plasma properties. In addition, turbulence models including electromagnetic effects and anomalous transport might be incorporated.

The diffusion approximation used for the radiation transport in this code has been shown to give agreement with exact integro-differential solutions for one-dimensional (axisymmetric) fields to a degree consistent with the accuracy by which the absorption properties of high-temperature air are known. The available higher-level approximations are therefore not under consideration for addition to XLIM3D at this time.[11]

#### Arc Path Modeling

Establishment of an arc path is not a simple matter. The MHD formulation yields an arc path that is diffuse and steady, whereas the actual arc is constricted and undergoes chaotic motion. An EMHD formulation, as described earlier, may result in a more accurate description of the arc.

Photos of the arc have been obtained at three locations along the constrictor. Typical results are shown in Fig. 7. As noted before, the dominant oscillations have displacements that cover a large fraction of the heater inside diameter. The arc does not remain on the centerline, and in fact, is quite close to the wall at times. To improve the arc heater lifetime, the arc should not approach the constrictor wall at any time. However, codes with conventional turbulence modeling will not predict an arc path with the degree of fluctuation shown in Fig. 7, and some modeling of the fluctuating arc path is necessary to understand and control the phenomena. Possible approaches to this modeling might be 1) use of some unconventional turbulence model, possibly including electromagnetic effects, 2) incorporate a vortex burst model, 3) use of a Monte Carlo technique, 4) apply some elements of lightning propagation theory, and 5) incorporate a theory of chaotic fluid motion.

## Summary

An arc heater development program has been undertaken to develop larger more capable arc heaters to satisfy some of the future hypersonic testing requirements. A new large arc heater (H3) has been operated successfully and is scheduled to be fully operational at chamber pressures up to 100 atm in 1996. Future plans also include the development of still higher pressure arc heaters and the development of a larger, higher power capability by manifolding several arc heaters into a single plenum or by developing a single very large arc heater. Analytical models have also been developed to assist in the design and development of arc heaters. Scaling laws and performance correlations in conjunction with basic computer codes such as SWIRLARC that predict overall performance have been valuable tools for arc heater development. The basic components of a three-dimensional arc heater code have been developed. It is built upon a three-dimensional Navier–Stokes code incorporating electromagnetic effects and a multidimensional radiation model. A near-electrode model has been developed that provides a more realistic description of the region where the arc passes from the air to the solid electrode than has previously been available. Water tunnel vortex breakdown work, when interpreted in conjunction with other experimental measurements such as photographs of the arc path, shows potential for interpretation of the phenomena occurring in the downstream end of the arc heater.

To broaden the base of knowledge of arc physics, improve heater reliability, and develop improved hardware designs, it is necessary to improve our understanding of the physical phenomena that occur inside the heater. Future modeling needs are as follows:

1) Complete the three-dimensional arc heater code; when mature, this code will provide an improved description of the details of arc heater phenomenology.

2) Further validate the near-electrode model by comparison with data from other types of arc heaters.

3) Develop an improved model for predicting and understanding arc stability. This may require an improved turbulence model or incorporating of a vortex burst model.

## Acknowledgments

The research reported herein was performed by the Arnold Engineering Development Center (AEDC), U.S. Air Force Materiel Command. Work and analysis for this research were done by personnel of Micro Craft Technology AEDC Operations, Technical Services Contractor for the AEDC aerospace flight dynamics facilities.

## References

[1]Bruce, W. E., III, and Horn, D. D., "AEDC Arc Column Diagnostic Measurements," *Proceedings of the 38th International Instrumentation Symposium* (Las Vegas, NV), 1992 (Paper 92-0190).

[2]Stewart, J. H., "AEDC-H2 Facility—New Test Capabilities for Hypersonic Air Breathing Vehicles," AIAA Paper 93-2781, July 1993.

[3]Horn, D. D., and Smith, R. T., "AEDC High-Enthalpy Ablation Test (HEAT) Facility Description, Development, and Calibration," Arnold Engineering Development Center, TR-81-10 (AD-A101747), July 1981.

[4]Horn, D. D., Felderman, E. J., and MacDermott, W. N., "Analysis and Results of External Magnetic Fields Applied to High Pressure DC Electric Arc Heaters," AIAA Paper 94-2040, June 1994.

[5]MacDermott, W. N., Horn, D. D., and Fisher, C. J., "Flow Contamination and Flow Quality in Arc Heaters Used for Hypersonic Testing," AIAA Paper 92-4028, July 1992.

[6]Felderman, E. J., Horn, D. D., Carver, D. B., and Davis, L. M., "AEDC Expanded Flow Arc Facility (HEAT-H2) Description and Calibration," *Proceedings of the 38th International Instrumentation Symposium* (Las Vegas, NV), 1992 (Paper 92-0191).

[7]Graves, C. M., Moody, H. L., Mitchell, J. D., and Horn, D. D., "Enthalpy Probe for Arc Heater Flow Diagnostics," AIAA Paper 93-2784, July 1993.

[8]MacDermott, W. N., Felderman, E. J., Sydor, M., and Gulhan, A., "Dimensional Analysis of Arc Heaters," AIAA Paper 95-2108, June 1995.

[9]Nicolet, W. B., Shepard, C. E., Clark, K. J., Balakrishnan, A., Kesselring, J. P., Suchsland, K. E., and Reese, J. J., Jr., "Analytical and Design Study for a High-Pressure, High-Enthalpy Constricted Arc Heater," Arnold Engineering Development Center, TR-75-47 (AD-A012551), July 1975.

[10]Shaeffer, J. F., "SWIRLARC: A Model for Swirling, Turbulent, Radiative Arc Heater Flowfields," *AIAA Journal*, Vol. 16, No. 10, 1978, pp. 1068–1075.

[11]Felderman, E. J., and MacDermott, W. N., "Radiative Heating in High-Pressure Arc Heaters," AIAA Paper 92-2873, July 1992.

[12]Reddy, K. C., and Benek, J. A., "A Locally Implicit Scheme for 3-D Compressible Viscous Flows," AIAA Paper 90-1525, June 1990.

[13]Felderman, E. J., Chapman, R., and Jacocks, J. L., "Development of a High-Pressure, High Power Arc Heater: Modeling Requirements and Status," AIAA Paper 94-2658, June 1994.

[14]Srinivasan, S., Tannehill, J. C., and Weilmuenster, K., "Simplified Curve Fits for the Thermodynamic Properties of Equilibrium Air," Iowa State Univ. of Science and Technology, ISU-ERI-Ames-88405, Ames, IA, Sept. 1987.

[15]Srinivasan, S., Tannehill, J. C., and Weilmuenster, K., "Simplified Curve Fits for the Thermodynamic Properties of Equilibrium Air," Iowa State Univ. of Science and Technology, ISU-ERI-Ames-86401, Ames, IA, June 1988.

[16]Baldwin, B. S., and Lomax, H., "Thin Layer Approximation and Algebraic Model for Separated Turbulent Flows," AIAA Paper 78-257, Jan. 1978.

[17]Nichols, R. H., "A Two-Equation Model for Compressible Flows," AIAA Paper 90-0494, Jan. 1990.

[18]Reddy, K. C., and Jacocks, J. L., "A Locally Implicit Scheme for the Euler Equations," AIAA Paper 87-1144, June 1987.

[19]Benek, J. A., Buning, P. G., and Steger, J. L., "A 3-D Chimera Grid Embedding Technique," AIAA Paper 85-1523, July 1985.

[20]Benek, J. A., Suhs, N. E., and Donegan, T. L., "Extended Chimera Grid Embedding Scheme with Application to Viscous Flows," AIAA Paper 87-1126, June 1987.

[21]Dietz, W. E., Jacocks, J. L., and Fox, J. H., "Application of Domain Decomposition to the Analysis of Complex Aerodynamic Configurations," *Proceedings of the 3rd International Symposium on Domain Decomposition Methods for Partial Differential Equations*, edited by T. F. Chan, R. Glowinski, J. Periaux, and O. B. Widlund, Society for Industrial and Applied Mathematics, Philadelphia, PA, 1990.

[22]Jameson, A., Schmidt, W., and Turkel, E., "Numerical Solutions of the Euler Equations by Finite Volume Methods Using Runge-Kutta Time Stepping Schemes," AIAA Paper 81-1259, June 1981.

[23]Swanson, R. C., and Turkel, E., "Artificial Dissipation and Central Difference Schemes for the Euler and Navier-Stokes Equations," AIAA Paper 87-1107, June 1987.

[24]Vincenti, W. G., and Kruger, C. H., *Introduction to Physical Gas Dynamics*, Wiley, New York, 1965.

[25]Vu, B. T., and Gouldin, F. C., "Flow Measurements in a Model Swirl Combustor," AIAA Paper 80-76, Jan. 1980.

[26]Felderman, E. J., and MacDermott, W. N., "Near-Electrode Model with Nonequilibrium Ionization at 100 Atm," AIAA Paper 95-1993, June 1995.

[27]Vakili, A. D., "An Investigation of the Influence of Forced Disturbances on Arc Heater Flow," Final Rept., AF F40600-92-K-0001, Nov. 1993.

[28]Faler, J. H., and Leibovich, S., "Disrupted States of Vortex Flow and Vortex Breakdown," *Physics of Fluids*, Vol. 20, No. 9, 1977, pp. 1385–1400.

[29]Khorrami, M., and Grosch, C., "Temporal Stability of Multiple Cell Vortices," AIAA Paper 89-0987, March 1989.

[30]Vakili, A. D., and Eramo, R. S., "Influence of Forced Disturbances on the Vortex Core and the Vortex Burst," U.S. Air Force Office of Scientific Research Univ POS_210_9MG_056, Univ. of Tennessee Space Inst., Nashville, TN, Oct. 1989.

[31]Tennent, S. G., "Experimental Investigation of a Confined Vortex Flow," M.S. Thesis, Univ. of Tennessee, Nashville, TN, Dec. 1993.

[32]Rhodes, R., and Keefer, D., "Non-Equilibrium Modeling of Hydrogen Arcjet Thrusters," International Electric Propulsion Conf., Paper 93-1904, Sept. 1993.

[33]Butler, G. W., and King, D. Q., "Single and Two Fluid Simulations of Arcjet Performance," AIAA Paper 92-3104, July 1992.

[34]Miller, S. A., and Martinez-Sanchez, M., "Multifluid Nonequilibrium Simulation of Electrothermal Arcjets," AIAA Paper 93-2101, June 1993.

[35]Megli, T. W., Krier, H., Burton, R. L., and Mertogul, A. E., "Two Temperature Modeling of $N_2/H_2$ Arcjets," AIAA Paper 94-2413, June 1994.

[36]Mikellides, P., Turchi, P., and Roderick, N., "Application of MACH2 Code to Magnetoplasmadynamic Arcjets," AIAA Paper 92-3297, July 1992.

[37]Shankar, V., Hall, W. F., and Mohammadian, A. H., "A Time-Domain Differential Solver for Electromagnetic Scattering Problems," *Proceedings of the IEEE*, Vol. 77, No. 5, 1989, pp. 709–721.

[38]Curtis, J. T., and Tramel, R. W., "NEQPAK, The AEDC Thermochemical Non-Equilibrium Package—Theory and Use," Arnold Engineering Development Center TR-93-20, April 1994.